Running head: Gut-bone axis in HLA-B27 rats

Title: Gut Inflammation in HLA-B27 Transgenic Rats Alters The Monocyte Compartment And Its Osteoclastogenic Potential

Cecilia Ansalone PhD[1], Lotta Utriainen PhD[2], Simon Milling PhD[1] and Carl S. Goodyear PhD[1]

[1]University of Glasgow, Institute of Infection, Immunity and Inflammation, Glasgow UK

[2]Laboratory of Immunology, National Eye Institute, National Institutes of Health, Bethesda, MD 20892, USA

Address correspondence to:

Dr. Carl S. Goodyear

Sir Graeme Davies Building, 120 University Place

Glasgow, G12 8TA, Scotland, UK

Email: Carl.Goodyear@glasgow.ac.uk

ABSTRACT

Objective

To investigate the relationship between intestinal inflammation and the central and peripheral innate immune system, in the pathogenesis of HLA-B27 associated spondyloarthritis.

Methods

The myeloid compartment of the bone marrow and blood of HLA-B27 transgenic (B27), control HLA-B7 transgenic (B7), and non-transgenic rats were evaluated by flow cytometry. Plasma from rats were assessed by ELISA for CCL2 and IL-1α levels. Rats were treated for 4 weeks with antibiotics and the blood and bone marrow myeloid compartments were evaluated by flow cytometry. The osteoclastogenic potential of bone marrow cells from antibiotic treated rats, in the presence or absence of TNFα, was evaluated *in vitro*.

Results

B27 rats have substantially higher numbers of circulating $Lin^{-}CD172a^{+}CD43^{lo}$ monocytes than control animals, which significantly correlates with higher levels of plasma CCL2. Antibiotic treatment of B27 rats markedly reduced ileitis, plasma CCL2 and IL-1α levels, and the number of bone marrow and blood $Lin^{-}CD172a^{+}CD43^{lo}$ monocytes, which have the greatest *in vitro* osteoclastogenic potential. Antibiotic treatment also prevented the TNFα-dependent enhancement of osteoclastogenesis in transgenic B27 rats.

Conclusions

The microbiota-dependent intestinal inflammation in B27 rats directly drives the systemic inflammatory and bone erosive potential of the monocyte compartment.

Introduction

The HLA-B27 allele of MHC class I (B27) is a major risk factor for the development of human spondyloarthritis (SpA), however, its exact contribution to disease enhancement is poorly understood. Transgenic rats that express the human HLA-B27 and β_2-microglobulin genes (B27 rats) develop multi-systemic inflammation that resembles the human SpA clinical spectrum(1,2). Inflammation in B27 rats starts in the intestine, with ileitis occurring before 10 weeks of age, followed by arthritis, psoriasis, and nail dystrophy(2). A link between gut pathology and peripheral symptoms has been known for decades, as animals raised in germ-free conditions develop neither colitis nor arthritis(3). There has been renewed interest in the intestinal environment and its contribution to the development of B27-associated pathology. It is now evident that the intestinal microbiome in B27 rats is profoundly different from that of healthy animals(4). Importantly, the development of gut pathology in B27 rats is associated with specific strains of commensal bacteria (i.e., *Bacteroides vulgatus*), which can be manipulated by oral antibiotic treatment(5,6). The impact of microbial dysbiosis on the central and systemic immune system, and the subsequent effect of this on disease development is currently under investigation. Recent work in mice has shown that acute *T. gondii*-driven intestinal inflammation can trigger changes in the bone marrow (BM) compartment, specifically BM monocyte precursor cells; fundamentally altering their function once they migrate into infected mucosal tissue(7). Interestingly, B27 animals lack MHC class II^{+} CD103^{+}CD172a^{low} migrating dendritic cells, which are involved in controlling intestinal immune responses(8). Furthermore, osteoclast pre-cursors in B27 rats have enhanced differentiation in response to TNFα compared to control animals, which contributes to the B27-associated bone loss(9). It still remains to be determined, however, how changes in the myeloid compartment, and B27-associated microbial dysbiosis, affect the central and peripheral myeloid compartments, and the osteoclast they mature into.

Herein, we have characterised monocyte populations in B27 rats and investigated the effects of oral antibiotics on both intestinal pathology and the myeloid compartment. We have revealed close correlations between gut pathology and monocyte distribution and showed how the latter could directly contribute to B27-associated bone loss.

Materials and Methods

Animal studies.

Heterozygous B27 and B7 PVG rats were bred under license as previously described(3,8), maintained under specific pathogen–free conditions at the University of Glasgow, and used under licenses issued by the UK Home Office. All rats were used between 10-18 weeks of age.

In vivo antibiotic treatment.

Rats between 10-14 weeks of age were given 50mg/kg/day of Vancomycin and 2.5mg/kg/day of Ampicillin/Metranidazole/Neomycin re-suspended in filtered sterile drinking water. Administration was by gavage daily on weekdays for 4 consecutive weeks (ABX treated group). Equal volume of sterile drinking water was given to control rats (CTRL). Blood was sampled twice a week from the tail vein and plasma stored. At day 26, animals were culled and blood, hind limbs and gut were harvested for downstream analysis.

Flow cytometry.

The white cell fraction of fresh isolated rat BM and blood was obtained by lysis of red cells using ACK lysing buffer (Life Technologies), and stained with fluorochrome-labelled antibodies and/or with biotinylated antibodies and fluorochrome-labelled streptavidin. Briefly, Fcγ receptor was blocked using purified mouse anti-rat CD32 (D34-485; BD Biosciences) and cells were stained with biotinylated mouse anti-rat Ig κ, CD90 (OX-6), CD45RA (OX-33), and brilliant violet 605^{TM} (BV650) Streptavidin (BioLegend). Monocytes

were identified using PE-CD172a (OX-41; BioLegend), APC-CD43 (W3/13; BioLegend), V450 or FITC-CD11b (WT.5; BD Biosciences). A DAPI solution (4',6-diamidino-2-phenylindole; Sigma-Aldrich) was used for live/dead cell exclusion. Cells were acquired using an LSRII analyser (BD Biosciences) and data analysed using FlowJo software (Tree Star).

Flow cytometry sorting of bone marrow cells.

Fluorescent-labelled cells were acquired and sorted using an Aria I sorter and a 70µm nozzle (BD Bioscience). Cells were sorted into tubes containing complete α-MEM media (supplemented with 10% FBS, 0,02 mM L-glutamine, 10 U/ml Penicillin, and 0.1 µg/ml Streptomycin; Invitrogen, Thermo Fisher Scientific) and kept a 4ºC till sorting completion. Purity of post-sorting test showed purity ≥ 96%. Sorted cells were seeded in 96 well plates at $1x10^6$ cells/ml and incubated overnight with 50 ng/ml M-CSF (PeproTech). On day 1, cells were stimulated with 50 ng/ml RANK-L (PeproTech). Medium was refreshed on day 4 and on day 6-7 cells were fixed and stained for tartrate-resistant acid phosphatase (TRAP) using the Acid Phosphatase TRAP kit, following the manufacturer's instructions (Sigma-Aldrich). Four representative images were acquired per well at 10X magnification using an EVOS® FL Auto Cell Imaging System (Life Technologies). Osteoclasts were identified as $TRAP^+$ (purple) cells with ≥3 nuclei and counted using Fiji software (Image J).

Uptake of fluorescent CCL2.

The fluorescent uptake of CCL2 toward CCR2 receptor was measured using Site-specific AF647® labelled chemokine purchased from ALMAC Group LTD, as previously described(10). Briefly, fresh primary cells were incubated at 37°C for 1h with 25 nM $CCL2^{AF647}$. Cells were then washed and stained for surface marker expression for flow cytometry.

Chemotaxis assay.

BM was collected from age-matched B7 and B27 rats. BM cells (BMCs) were suspended at $5x10^6$ cells/ml in chemotaxis buffer (Dulbecco modified essential medium (DMEM) supplemented with 0.5% BSA; Life technology, Thermo Fisher Scientific) and 100 µl of the cell suspension was placed onto the top section of a bare filter trans-well (6.5 mm diameter) with 5 µm pore size (Corning, UK). Rat CCL2 (0, 10, 100 and 1000 ng/ml) was used as a chemo-attractant in the bottom section of the trans-wells (PeproTech). After 3 hours of incubation at 37ºC, trans-migration was assessed by counting the cells that had migrated into the bottom section of the well. Transmigrated cells were further collected and stained for flow cytometry.

Enzyme-linked immunosorbent assay (ELISA)

Blood was collected in heparinised tubes and plasma stored; rat CCL2 and IL-1α were measured by ELISA following the manufacturer's instructions (BioLegend and Thermo Fisher Scientific respectively).

Rat bone marrow-derived monocyte collection and osteoclastogenesis.

Briefly, BM was flushed from long bones and red cells lysed with ACK lysing buffer (Life Technologies). BMCs were cultured at $1x10^6$ cells/ml in α-MEM media (supplemented with 10% FBS, 0,02 mM L-glutamine, 10 U/ml Penicillin, and 0.1 µg/ml Streptomycin; Invitrogen, Thermo Fisher Scientific) in the presence of 2.5 mM β-glycerophosphate and 0.05 mg/ml L-Ascorbic Acid (Sigma-Aldrich) for 2 days. After incubation, non-adherent BMCs (NA-BMCs) were collected, seeded at $2x10^5$ cells/well in 96 well plates, and cultured in triplicate in the presence of 50 ng/ml M-CSF, 10 ng/ml RANK-L, and 50 ng/ml TNFα (PeproTech). Medium was refreshed on day 4 and on day 5 cells were fixed, stained for TRAP, and osteoclast quantified, as described above.

Rat gut: tissue processing, haematoxylin and eosin staining, and analysis

Several pieces of the ileum were collected from rats under terminal anaesthesia (4 atm Isoflourane and 4 atm O_2) and fixed in 4% neutral buffered formalin. Samples were dehydrated via increasing concentrations of ethanol and embedded in paraffin wax blocks. Transversal and cross sections were cut at 5 μm using a microtome and stained for haematoxylin and eosin and mounted with DPX mountant (Sigma-Aldrich Chemical Co.). Stained sections were imaged using an EVOS® FL Auto Cell Imaging System (Life Technologies) with a 10X objective. Villi and crypt length were measured using a Fiji software (ImageJ).

Statistical analysis

Prism 6 (Graphpad) was used to perform all statistical analysis and statistical tests used are indicated in the figure legends. For all statistical analysis, p-values of ≤0.05 were considered significant.

Results

B27 rats have an altered myeloid compartment with increased CD43^{lo} monocytes

Rat monocytes (M_Os) within the blood and BM(11,12) were identified as lin$^-$ (Igκ$^-$CD90$^-$OX-33$^-$) SSC^{lo}CD172a^{hi} and sub-divided by expression of CD43 (Supplemental Figure 1). As previously reported(11), the majority of circulating M_Os in healthy WT rats were CD43^{hi} (75.3±7.0%). B27 rats had a significantly altered ratio of CD43^{lo}:CD43^{hi} M_Os; with 44.2±12.7% CD43^{lo} and only 54.0±11.5% CD43^{hi} (Figure 1A-B). This change corresponded with a substantially higher number of circulating CD43^{lo} M_Os in B27 animals (Figure 1C). Interestingly, CD43^{hi} M_O numbers were not significantly affected in B27 rats (Figure 1C). This increased representation of CD43^{lo} M_Os was also observed within the BM of B27 rats

when compared to WT and B7 transgenic controls (Figure 1D-F). Importantly, no differences were evident between WT and the B7 transgenic controls (Figure 1).

Antibiotics reduce the number of circulating CD43^{lo} monocytes by restoring CCL2 plasma levels and reducing BM pre-cursor numbers.

Oral antibiotics are effective at attenuating signs of ileitis in B27 rats(6). Using broad-spectrum antibody treatment, we ameliorated B27-associated gut inflammation; as determined by reduced ileitis after 4 weeks of oral administration (Figure 2A-B). Surprisingly, this was associated with a reduction in CD43^{lo} M$_O$s not only within the bloodstream but also within the BM of B27 rats (Fig. 2C-F). This antibiotic-induced modulation of monocyte composition did not occur in control animals; as treated and un-treated non-transgenic animals had comparable numbers of M$_O$s.

Rat CD43^{lo} M$_O$s express CCR2(11), which is a key chemokine receptor involved in monocyte migration from the BM into the bloodstream and recruitment into inflamed tissues. We confirmed CCR2 expression in CD43^{lo} M$_O$s using fluorescently-labelled CCL2 (Figure 3A) and migration towards CCL2 (Figure 3B). Additionally, we observed significantly higher CCL2 plasma levels in B27 rats compared to controls (Figure 3C). These data indicate that there may be CCL2-dependent altered migration/recruitment of M$_O$s in B27-associated diseases. This is supported by a significant positive correlation between CCL2 plasma levels and the number of circulating CD43^{lo} M$_O$s in B27 rats (Figure 3D). Moreover, administration of antibiotics to B27 rats significantly decreased the plasma levels of CCL2 (Figure 3E). Remarkably, one week after initiation of antibiotics, plasma CCL2 in B27 rats returned to levels similar to WT controls (Figure 3E). Furthermore, we evaluated whether or not the antibiotic treatment affected systemic cytokines in B27 rats. TNFα is known to be highly linked to B27-associated disease, however, it was undetectable in both plasma and serum (data not shown). In contrast, the level of IL-1α (a potent pro-inflammatory cytokine often

associated with TNFα activity) was significantly higher in the plasma of B27 rats compared to controls (Figure 3F). Notably, IL-1α plasma levels in B27 rats substantially decreased following antibiotic treatment (Figure 3G). These data indicate that oral antibiotics not only reduces local inflammation in the gut but also have an impact on systemic inflammation by reducing circulating levels of IL-1α, CCL2, and $CD43^{lo}$ M_Os.

Oral antibiotic treatment re-establishes normal responsiveness to TNFα within the BM pre-osteoclast compartment of B27 rats

Recent studies have shown that murine monocyte sub-populations have different osteoclastogenic potential(13). Evaluation of the osteoclastogenic potential of each of the rat BM monocyte populations revealed that the $CD43^{lo}$ M_O population contains the main osteoclast pre-cursors (Figure 4). Therefore, the observed increase in this population in B27 rats could contribute to the overt bone pathology observed in these animals as they age. Furthermore, it has been demonstrated that BM pre-cursors from B27 rats undergo enhanced TNFα-driven (but not RANK-L) osteoclastogenesis compared to controls(9) (Supplemental Figure 2). Moreover, the TNFα-enhancement of OC differentiation in B27 rats has been associated with IL-1α production and activity(9), which is reduced in the plasma of B27 animals upon treatment with oral antibiotics (Figure 3F). Importantly, the restoration of homeostasis within the monocyte compartment in B27 BM after antibiotics (Figure 2) also reversed the TNFα-dependent enhancement of osteoclast differentiation in these animals (Figure 5). Thus, treatment of B27 rats with oral antibiotics not only resolves their microbiota-dependent intestinal inflammation, but also reduced the levels of circulating CCL2, restored homeostasis to blood and BM M_Os, and reversed defects in osteoclasts generated from these monocytes.

Discussion

It is becoming increasing apparent that the microbial environment within the gut is relevant to not only intestinal pathologies but also rheumatic diseases (i.e., RA and AS)(14). Over-expression of HLA-B27 and β_2-microglobulin in rats leads to multi-systemic SpA-like inflammation that starts within the gut(1) and is associated with intestinal dysbiosis in early stages of disease development(4,15). These animals provide a model to examine mechanisms of microbial-mediated systemic inflammation and bone disease, which are also observed in HLA-B27$^+$ axSpA patients who are often reported to have subclinical intestinal inflammation(16).

Intestinal inflammation in B27 animals leads to increased systemic levels of CCL2; this is associated with higher numbers of CCR2$^+$CD43^{lo} M$_O$s in both the BM and peripheral blood. The CCL2/CCR2 interaction is known to regulate monocyte release from the BM, where they are generated, into the bloodstream(17). Perturbation of both CCL2 and CCR2 has been associated with impaired emigration of BM-M$_O$s into the bloodstream and thus lower numbers of circulating 'classical' CCR2$^+$ M$_O$s in steady-state and during inflammation(18,19). How peripheral inflammation can lead to increased CCL2 production and monocyte recruitment is still under debate. However, it is known that low concentrations of TLR ligands in the blood induce CCL2 production within the BM, which corresponded to an enhanced migration of CCR2$^+$ M$_O$s into the bloodstream(20). Thus, an increase in the amounts of microbial molecules absorbed across the intestinal barrier might contribute to the initiation and progression of inflammatory responses. We, therefore, suggest that intestinal inflammation in B27 rats can facilitate the dysregulation of the monocyte compartment by inducing increased CCL2 expression during the development and perpetuation of disease. This is supported by the fact that antibiotic treatment not only reduces the B27 intestinal inflammation but also normalises CCL2 levels and monocyte frequencies. Interestingly,

'classical' M_Os are generated within the BM and when released into the bloodstream they represent an obligatory intermediate state for the differentiation of 'patrolling' M_Os(11,21). We observed a disconnect in this normal process in the B27 rats, with higher levels of 'classical' $CD43^{lo}$ M_Os that persist in both the central (BM) and peripheral compartment. The observed changes in M_Os in B27 rats have important implications for bone disease as we have demonstrated that the $CD43^{lo}$ M_Os are the major pre-cursors for osteoclasts in rats. Furthermore, our data are consistent with the recent observation that B27 rats have pronounced increased osteoclastogenic potential only in the presence of TNFα(9). These data taken together may indicate that the B27-osteoclast phenotype directly results from an increase in the frequency of the $CD43^{lo}$ M_O pre-cursors in B27 animals. This interpretation is supported by the fact that antibiotic treatment reduces intestinal inflammation, systemic CCL2 levels, numbers of BM and circulating $CD43^{lo}$ M_Os, and reverses the B27-associated TNFα enhanced osteoclastogenesis. Interestingly, previous studies have shown that anti-TNFα treatment can inhibit both intestinal inflammation and enthesitis in the peripheral joints of B27 animals(22), however, the impact on $CD43^{lo}$ M_O pre-cursors was not evaluated. It would therefore be interesting to determine whether or not anti-TNFα treatment recapitulates those changes seen with antibiotic treatment.

One limitation of our study is that we were not been able to show the *in vivo* consequences of antibiotic treatment on bone pathology. However, it is important to note that the B27 rats used in this study were not old enough to show overt signs of bone pathology. This includes no observable changes in circulating bone turnover markers (i.e., collagen type 1 cross-linked C-telopeptide and procollagen type 1 N-terminal propeptide), osteoclast number at bone surfaces, or bone architecture via microCT (data not shown). Studies in our laboratory have only been able to detect increased osteoclast numbers at bone surfaces and changes in bone architecture in B27 rats that are a minimum of 36 weeks old (data not

shown). Thus, further studies are required to evaluate the long-term impact of antibiotic treatment on bone pathology in this model.

In terms of human disease, alteration in the peripheral monocyte pool has also been found in axSpA patients. These patients have higher frequencies of classical $CD14^{hi}CD16^{-}$ monocytes, which correspond to the $CD43^{lo}$ monocytes in the rat. This higher frequency of classical monocytes has been associated with spontaneous and elevated production of pro-inflammatory cytokines in axSpA patients under conventional therapy but not under anti-TNFα biologics, and this also correlated with BASDAI(23). Together these data support a direct and important role of classical monocytes in disease progression. However, further studies are still needed to assess the interaction between gut inflammation, the myeloid compartment, and the resulting clinical disease. Recent studies have also started to address dysbiosis in rheumatic diseases; revealing alteration in the intestinal microbiome in early RA(24-25), axSpA(26-27), and PsA(28). However, once again more work is required to understand the impact of intestinal perturbation on systemic pathology in remote sites such as the joints and bone. Notably, recent studies have shown that gut dysbiosis in PsA patients correlates with a lower concentration of medium-chain fatty acids (MCFAs) and RANK-L, which have protective effects in maintaining the mucosal integrity and promoting DC/OC differentiation in the intestinal lumen respectively(28). Supporting the concept that there is a potential link between gut dysbiosis/inflammation and the osteoclast compartment in PsA patients.

In conclusion, we have shown that modulation of the intestinal microbiota in an animal model of axSpA not only has wide-ranging effects on systemic inflammatory cells and soluble mediators, but also on osteoclastogenesis. This raises the possibility that manipulation of the intestinal microbiota in patients with axSpA may provide clinical benefits by restoring homeostasis to both the immune and skeletal systems.

Acknowledgements.

The authors would like to thank D. Vaughan for flow cytometry support, J. Reilly and S. Kerr for Immunohistochemistry support, and Dr T Zangerle Murray for technical assistance with preparation of gut samples. This research was supported by the Seventh Framework Programme and Marie Curie Actions (European Commission, FP7-PEOPLE-2011-ITN-289150 "Osteoimmune").

Contributions

C.A, S.M, and C.S.G conceived the study, planned and reviewed experiments, analyzed the data and wrote the paper. L.U, and C.A performed experiments.

Declaration of interests

Authors report no competing financial interests.

References

1. Hammer RE, Maika SD, Richardson JA, Tang JP, Taurog JD. Spontaneous inflammatory disease in transgenic rats expressing HLA-B27 and human beta 2m: an animal model of HLA-B27-associated human disorders. *Cell* 1990;63:1099–1112.

2. Taurog JD, Maika SD, Simmons WA, Breban M, Hammer RE. Susceptibility to inflammatory disease in HLA-B27 transgenic rat lines correlates with the level of B27 expression. *J Immunol* 1993;150:4168–4178.

3. Taurog JD, Richardson JA, Croft JT, Simmons WA, Zhou M, Fernández-Sueiro JL, et al. The germfree state prevents development of gut and joint inflammatory disease in HLA-B27 transgenic rats. *J Exp Med* 1994;180:2359–2364.

4. Lin P, Bach M, Asquith M, Lee AY, Akileswaran L, Stauffer P, et al. HLA-B27 and Human β2-Microglobulin Affect the Gut Microbiota of Transgenic Rats. Bereswill S, ed. *PLoS ONE* 2014;9:e105684.

5. Rath HC, Herfarth HH, Ikeda JS, Grenther WB, Hamm TE, Balish E, et al. Normal luminal bacteria, especially Bacteroides species, mediate chronic colitis, gastritis, and arthritis in HLA-B27/human beta2 microglobulin transgenic rats. *J Clin Invest*

1996;98:945–953.

6. Rath HC, Schultz M, Freitag R, Dieleman LA, Li F, Linde HJ, et al. Different subsets of enteric bacteria induce and perpetuate experimental colitis in rats and mice. *Infect Immun* 2001;69:2277–2285.

7. Askenase MH, Han S-J, Byrd AL, da Fonseca DM, Bouladoux N, Wilhelm C, et al. Bone-Marrow-Resident NK Cells Prime Monocytes for Regulatory Function during Infection. *Immunity* 2015;42:1130–1142.

8. Utriainen L, Firmin D, Wright P, Cerovic V, Breban M, McInnes I, et al. Expression of HLA-B27 causes loss of migratory dendritic cells in a rat model of spondylarthritis. *Arthritis & Rheumatology* 2012;64:3199–3209.

9. Layh-Schmitt G, Yang EY, Kwon G, Colbert RA. HLA-B27 Alters the Response to Tumor Necrosis Factor α and Promotes Osteoclastogenesis in Bone Marrow Monocytes From HLA-B27-Transgenic Rats. *Arthritis & Rheumatology* 2013;65:2123–2131.

10. Ford LB, Cerovic V, Milling SWF, Graham GJ, Hansell CAH, Nibbs RJB. Characterization of Conventional and Atypical Receptors for the Chemokine CCL2 on Mouse Leukocytes. *The Journal of Immunology* 2014;193:400–411.

11. Yrlid U, Jenkins CD, MacPherson GG. Relationships between distinct blood monocyte subsets and migrating intestinal lymph dendritic cells in vivo under steady-state conditions. *J Immunol* 2006;176:4155–4162.

12. Barnett-Vanes A, Sharrock A, Birrell MA, Rankin S. A Single 9-Colour Flow Cytometric Method to Characterise Major Leukocyte Populations in the Rat: Validation in a Model of LPS-Induced Pulmonary Inflammation. Sanchez-Margalet V, ed. *PLoS ONE* 2016;11:e0142520.

13. Charles JF, Hsu L-Y, Niemi EC, Weiss A, Aliprantis AO, Nakamura MC. Inflammatory arthritis increases mouse osteoclast precursors with myeloid suppressor function. *J Clin Invest* 2012;122:4592–4605.

14. Bravo-Blas A, Wessel H, Milling S. Microbiota and arthritis. *Current Opinion in Rheumatology* 2016:1.

15. Jacques P, Elewaut D. Joint expedition: linking gut inflammation to arthritis. *Mucosal Immunology* 2008;1:364–371.

16. Van Praet L, Van den Bosch FE, Jacques P, Carron P, Jans L, Colman R, et al. Microscopic gut inflammation in axial spondyloarthritis: a multiparametric predictive model. *Annals of the Rheumatic Diseases* 2013;72:414–417.

17. Serbina NV, Pamer EG. Monocyte emigration from bone marrow during bacterial infection requires signals mediated by chemokine receptor CCR2. *Nat Immunol* 2006;7:311–317.

18. Tsou C-L, Peters W, Si Y, Slaymaker S, Aslanian AM, Weisberg SP, et al. Critical roles for CCR2 and MCP-3 in monocyte mobilization from bone marrow and recruitment to inflammatory sites. *J Clin Invest* 2007;117:902–909.

19. Jia T, Serbina NV, Brandl K, Zhong MX, Leiner IM, Charo IF, et al. Additive roles for MCP-1 and MCP-3 in CCR2-mediated recruitment of inflammatory monocytes during Listeria monocytogenes infection. *J Immunol* 2008;180:6846–6853.

20. Shi C, Jia T, Mendez-Ferrer S, Hohl TM, Serbina NV, Lipuma L, et al. Bone Marrow Mesenchymal Stem and Progenitor Cells Induce Monocyte Emigration in Response to Circulating Toll-like Receptor Ligands. *Immunity* 2011;34:590–601.

21. Yona S, Kim K-W, Wolf Y, Mildner A, Varol D, Breker M, et al. Fate Mapping Reveals Origins and Dynamics of Monocytes and Tissue Macrophages under Homeostasis. *Immunity* 2013;38:79–91.

22. Milia AF, Manneschi LI, Manetti M. Evidence for the prevention of enthesitis in HLA-B27/hβ2m transgenic rats treated with a monoclonal antibody against TNF-α. *Journal of Cellular and Molecular Medicine*. 2011;15:270-279.

23. Conrad K, Wu P, Sieper J, & Syrbe U. In vivo pre-activation of monocytes in patients with axial spondyloarthritis. *Arthritis Res & Ther 2015*; 16;17:179.

24. Eerola E, Mottonen T, Hannonen P, et al. Intestinal flora in early rheumatoid arthritis. *Br J Rheumatol*. 1994;33:1030–8.

25. Vaahtovuo J, Munukka E, Korkeamaki M, Luukkainen R, Toivanen P. Fecal microbiota in early rheumatoid arthritis. *The Journal of Rheumatology*. 2008;35:1500–5.

26. Stebbings S, Munro K, Simon MA, et al. Comparison of the faecal microflora of patients with ankylosing spondylitis and controls using molecular methods of analysis. *Rheumatology*. 2002;41:1395–401.

27. Costello ME, Ciccia F, Willner D, et al. Intestinal dysbiosis in ankylosing spondylitis. *Arthritis & Rheumatology*. 2014; 67(3):686-691.

28. Scher JU, Ubeda C, Artacho A, et al. Decreased bacterial diversity characterizes the altered gut microbiota in patients with psoriatic arthritis, resembling dysbiosis in inflammatory bowel disease. *Arthritis & Rheumatology* 2015; 67:128–39.

Figure Legends:

Figure 1. B27 rats have increased CD43^{lo} monocytes in the bone marrow and blood. (A-F) The white fraction of cells was collected from WT, B7, and B27 blood and bone marrow (BM) and analysed via flow cytometry. **(A)** Representative density plots showing the expression of CD11b and CD43 of circulating blood monocytes (M_Os; lin$^-$SSC^{lo}CD172a$^+$) in

WT and B27 animals. The experiment was repeated 3 times for a total of n=6 for each group; in **(B)** the percentage and in **(C)** the absolute numbers of $CD43^{lo}$ and $CD43^{hi}$ in WT, B7 and B27 determined. **(D)** BM was collected from WT, B7 and B27 rats and analysed for the expression of CD172a and CD43. Representative density plots show the distribution of BM M_Os in B7 and B27 rats. **(E)** Percentages and **(F)** absolute numbers of the M_O subsets in WT, B7 and B27 animals. Numbers were calculated from three different experiments pooled together for a total of n=5 for WT and n=6 for B7 and B27. Data were analysed using 2-way ANOVA with Tukey's multiple comparisons test. *=P<0.05; **=P≤0.005. ***= P≤0.001. ****= P≤0.0001.

Figure 2. Antibiotics reduce ileitis and re-establish normal levels of $CD43^{lo}$ monocytes in B27 animals. (A-F) B27 and WT animals received 4 weeks of antibiotics (ABX) or water (vehicle control, CTRL) and at day 26 the blood white cell fraction and bone marrow cells (BMCs) were collected and stained for flow cytometry. **(A)** Representative H&E staining sections of the ileum of ABX and water-treated (CTRL) WT or B27 rats. Tissue sections were visualised and digital images captured using an EVOS FL Auto Cell Imaging System with a 10X objective. Scale bars = 400 μm. **(B)** Quantification of villus to crypt ratio. For each sample the average of the length of villus and crypt was calculated on 2 different tissue sections. Error bars show mean ± SD of n=3-4 for ABX and n=2-3 for CTRL. **(C)** Representative flow cytometry plots showing the monocyte gating in CTRL and ABX within the blood. **(D)** Quantification of circulating $CD43^{lo}$ and $CD43^{hi}$ M_Os in B27 and WT rats receiving ABX or water (CTRL). **(E)** Representative dot plots show the BM monocyte populations in CTRL and ABX B27 rats. **(F)** Quantification of $CD43^{lo}$ and $CD43^{hi}$ subsets. **(D&F)** Numbers were calculated from 3 different experiments pooled together using B27 (n=9 for B27-CTRL and n=12 for B27-ABX) and one experiment using WT rats (n=3). Data

were analysed using Kruskal-Wallis test with Dunn's post hoc test in **(B)** and one-way ANOVA in **(D&F)** with Sidak's multiple comparison test. *=$P \leq 0.05$; **=$P \leq 0.005$; ***=$P \leq 0.0005$.

Figure 3. Antibiotics reduce CCL2 plasma levels in B27 rats. (A-B) $CD43^{lo}$ monocytes uptake CCL2 and efficiently migrate toward CCL2 gradient. **(A)** Blood and BM cells were collected from WT rats, incubated with $CCL2^{AF647}$ followed by staining for surface marker expression and flow cytometry analysis. The representative histograms show $CCL2^{AF647}$ fluorescence of $CD43^{lo}$ and $CD43^{hi}$ M_O subsets in blood and BM. The experiment used 3 different animals and showed comparable results. **(B)** BM was collected from a WT animal and total BMCs were placed in the top section of a bare filter trans-well. Increasing concentrations of recombinant rat CCL2 were used as chemo-attractant in the bottom section of the trans-wells. After 3 hours, trans-migrated cells were collected, stained and quantified via flow cytometry. Data were analysed with 2-way ANOVA and Dunnett's post-hoc test comparing each data set to the 0 ng/ml values. Data shown are from 1 experiment performed in triplicate. Bars show mean ± SD. *= $P \leq 0.05$; **= $P \leq 0.01$; ****= $P \leq 0.0001$. **(C)** Plasma was collected from B7 and B27 animals and CCL2 plasma levels quantified by ELISA. Data were analysed with Mann Whitney test. *= $P \leq 0.05$; n=6 for both B7 and B27 samples. **(D)** Blood from B27 animals receiving the vehicle (CTRL) was collected twice a week for 4 weeks; numbers of $CD43^{lo}$ and CCL2 plasma levels were measured for each sample. Samples were collected from 2 different experiments and results pooled. Correlation analysis was performed using Pearson r test. n=50. **(E)** Plasma was collected at different time points (day 1 to 26) from B27 and WT rats treated with ABX or water (CTRL) and CCL2 measured by ELISA. Plasma CCL2 of 3 different experiments pooled together in B27 rats and 1 experiment using WT. Error bars shown mean ± SD. In B27-CTRL n=9; in B27-ABX n=12;

in WT-CTRL n=3; in WT-ABX n=3. Data were analysed using 2-way ANOVA and Sidak's multiple comparison test for repeated measure. *=$P \leq 0.05$; **=$P \leq 0.005$; ***=$P \leq 0.0005$. **(F)** IL-1α was measured in day 21 plasma samples from both WT and B27 groups. Error bars indicate mean ± SD of n=9-10 for B27 and n=3 for WT groups. Kruskal-Wallis test with Dunn's multiple comparisons test was used to assess the significance. **= $P \leq 0.01$.

Figure 4. $CD43^{lo}$ monocytes develop the highest number of osteoclasts *in vitro*. BMCs were collected from B7, B27 and WT rats and specific monocyte populations were sorted using flow cytometry. Sorted cells were cultured at the same density in pro-osteoclastogenic medium (50 ng/ml M-CSF and 50 ng/ml RANK-L) and after 7 days fixed and stained for TRAP. **(A)** Representative pictures of TRAP staining (purple staining) of the total BMCs and the different subpopulation analysed. Scale bar = 500μm **(B)** $TRAP^+$ multinucleated (≥3 nuclei) cells ($TRAP^+$ MNCs) were quantified as osteoclasts. Bars show mean ± SD. n=3 for WT, B7, and B27, from 3 different experiments pooled together.

Figure 5. Antibiotics reverse the BM monocyte/osteoclast phenotype of B27 animals. B27 and WT animals received 4 weeks of ABX or water (CTRL) and at day 26 non-adherent-BMCs were collected and cultured in presence of 50 ng/ml M-CSF, 10 ng/ml RANK-L, and 50 ng/ml TNFα in triplicate wells. On day 4, medium was refreshed and on day 5 cells were fixed and stained for TRAP. Osteoclasts were quantified as $TRAP^+$ MNCs (≥3 nuclei) from 4 digital pictures per well. **(A)** The number of $TRAP^+$ MNCs deriving from culture of B27 and WT ABX and CTRL animals. Data in B27 derived from 2 different experiments pooled together for a total of n=7-8 for B27 and n=3 for WT. **(B)** Representative pictures show TRAP staining in a CTRL and ABX B27 cultures. Data were analysed with one-way ANOVA and Sidak's multiple comparison test. *=$P \leq 0.05$. **=$P \leq 0.005$.

Supplemental Figure 1. Gating strategy for the identification of monocytes and monocyte subsets within the blood and BM. White cell fraction was collected from blood **(A)** and BM **(B)** of WT rats, stained for flow cytometry, and analysed. **(A-B)** Representative flow cytometry plots show the gating strategy used to identify monocyte subsets. Single $DAPI^-$ cells were identified as live cells and further gated. Ig kappa (Igκ), CD90, and OX-33 (CD45RA) were used to exclude B and T cells from the analysis. Polymorphonuclear cells (PMNs) and monocytes (M_Os) were gated by their side scatter properties (SSC-A) and expression of CD172a. M_Os ($SSC^{lo}CD172a^{hi}$) were further analysed by their expression of CD11b and CD43. **(A)** Within the blood two different populations were gated: $CD11b^+CD43^{lo}$ (or $CD43^{lo}$) and $CD11b^+CD43^{hi}$ (or $CD43^{hi}$). **(B)** $CD43^{hi}$ and $CD43^{lo}$ in the BM were gated based on the expression of CD172a. Numbers in the density plots indicates frequencies of the parent population.

Supplemental Figure 2. TNFα/RANK-L synergism in osteoclastogenesis is enhanced in B27 animals. BMCs were collected from age matched WT, B7, and B27 rats and incubated for 2 days with 2.5 β-glycerol phosphate and 0.05 mg/ml L-ascorbic acid. On day 1 NA-BMCs were collected and plated in the presence of 50 ng/ml M-CSF and 10 ng/ml RANK-L, and different concentrations of TNFα (10, 50 or 100 ng/ml). Cells were fixed and stained for TRAP on day 5. **(A)** Representative reconstructed pictures of TRAP stained cultures from a B7, and B27 NA-BMCs treated with varying TNFα concentrations. **(B)** Quantification of osteoclasts number ($TRAP^+$ MNCs) from four pictures per well taken at 10X magnification. Bars show mean ± SD of an n=3. Data were analysed with 2way ANOVA and Sidak's multiple comparisons test. *= $P \leq 0.05$. **= $P \leq 0.005$.

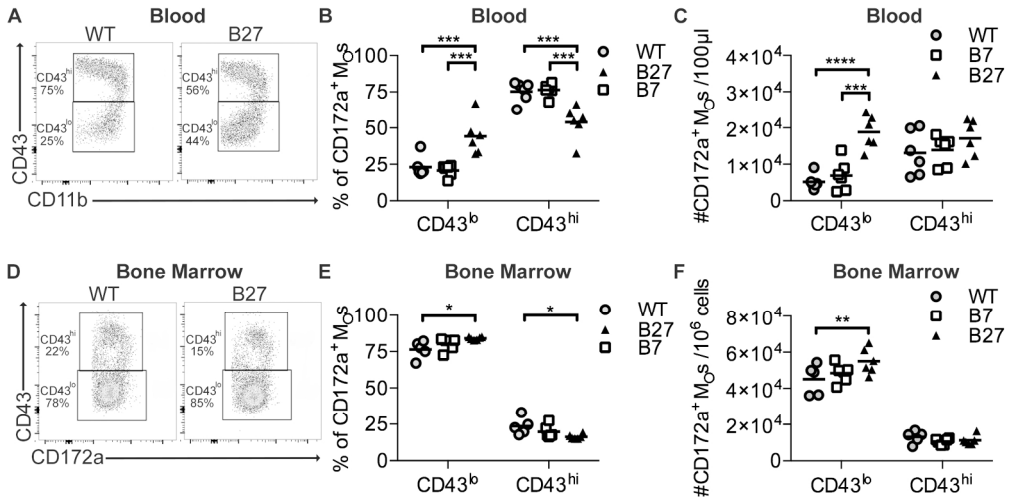

Figure 1. B27 rats have increased CD43lo monocytes in the bone marrow and blood. (A-F) The white fraction of cells was collected from WT, B7, and B27 blood and bone marrow (BM) and analysed via flow cytometry. **(A)** Representative density plots showing the expression of CD11b and CD43 of circulating blood monocytes (M_Os; $lin^-SSC^{lo}CD172a^+$) in WT and B27 animals. The experiment was repeated 3 times for a total of n=6 for each group; in **(B)** the percentage and in **(C)** the absolute numbers of $CD43^{lo}$ and $CD43^{hi}$ in WT, B7 and B27 determined. **(D)** BM was collected from WT, B7 and B27 rats and analysed for the expression of CD172a and CD43. Representative density plots show the distribution of BM M_Os in B7 and B27 rats. **(E)** Percentages and **(F)** absolute numbers of the M_O subsets in WT, B7 and B27 animals. Numbers were calculated from three different experiments pooled together for a total of n=5 for WT and n=6 for B7 and B27. Data were analysed using 2-way ANOVA with Tukey's multiple comparisons test. *=P<0.05; **=P≤0.005. ***= P≤0.001. ****= P≤0.0001.

177x90mm (300 x 300 DPI)

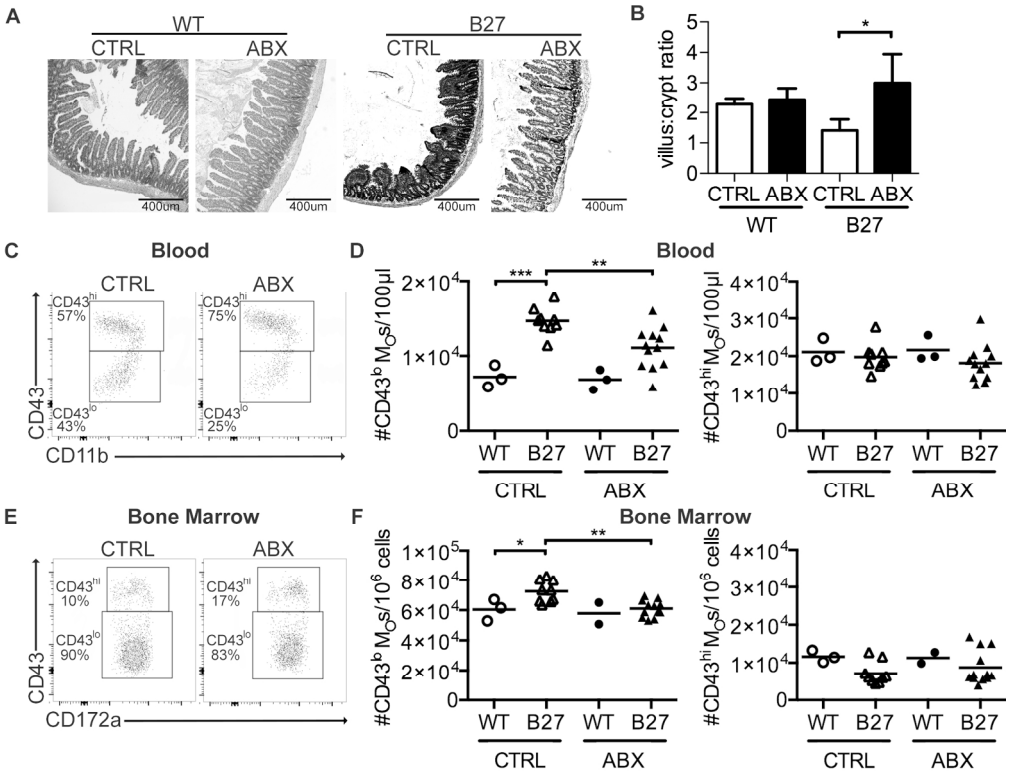

Figure 2. Antibiotics reduce ileitis and re-establish normal levels of CD43lo monocytes in B27 animals. (A-F) B27 and WT animal received 4 weeks of antibiotics (ABX) or water (vehicle control, CTRL) and at day 26 the blood white cell fraction and bone marrow cells (BMCs) were collected and stained for flow cytometry. **(A)** Representative H&E staining sections of the ileum of ABX and water-treated (CTRL) WT or B27 rats. Tissue sections were visualised and digital images captured using an EVOS FL Auto Cell Imaging System with a 10X objective. Scale bars = 400 µm. **(B)** Quantification of villus to crypt ratio. For each sample the average of the length of villus and crypt was calculated on 2 different tissue sections. Error bars show mean ± SD of n=3-4 for ABX and n=2-3 for CTRL. **(C)** Representative flow cytometry plots showing the monocyte gating in CTRL and ABX within the blood. **(D)** Quantification of circulating $CD43^{lo}$ and $CD43^{hi}$ MOs in B27 and WT rats receiving ABX or water (CTRL). **(E)** Representative dot plots show the BM monocyte populations in CTRL and ABX B27 rats. **(F)** The quantification of $CD43^{lo}$ and $CD43^{hi}$ subsets. **(D&F)** Numbers were calculated from 3 different experiments pooled together using B27 (n=9 for B27-CTRL and n=12 for B27-ABX) and one experiment using WT rats (n=3). Data were analysed using Kruskal-Wallis test with Dunn's post hoc test in **(B)** and one-way ANOVA in **(D&F)** with Sidak's multiple comparison test. *=P≤0.05; **=P≤0.005; ***=P≤0.0005.

170x129mm (300 x 300 DPI)

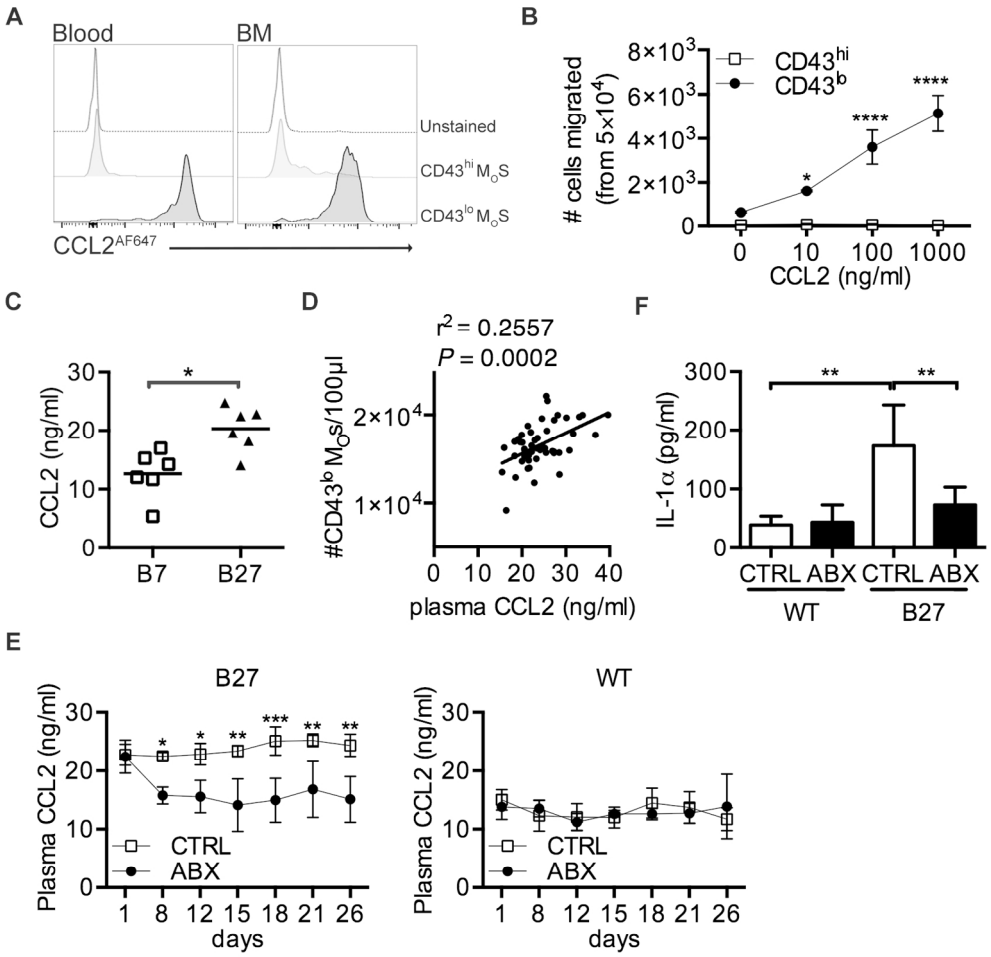

Figure 3. Antibiotics reduce CCL2 plasma levels in B27 rats. (A-B) CD43^{lo} monocytes uptake CCL2 and efficiently migrate toward CCL2 gradient. **(A)** Blood and BM cells were collected from WT rats, incubated with CCL2^{AF647} followed by staining for surface marker expression and flow cytometry analysis. The representative histograms show CCL2^{AF647} fluorescence of CD43^{lo} and CD43^{hi} M_O subsets in blood and BM. The experiment used 3 different animals and showed comparable results. **(B)** BM was collected from a WT animal and total BMCs were placed in the top section of a bare filter trans-well. Increasing concentrations of recombinant rat CCL2 were used as chemo-attractant in the bottom section of the trans-wells. After 3 hours, trans-migrated cells were collected, stained and quantified via flow cytometry. Data were analysed with 2-way ANOVA and Dunnett's post-hoc test comparing each data set to the 0 ng/ml values. Data shown are from 1 experiment performed in triplicate. Bars show mean ± SD. *= P≤0.05; **= P≤0.01; ****= P≤0.0001. **(C)** Plasma was collected from B7 and B27 animals and CCL2 plasma levels quantified by ELISA. Data were analysed with Mann Whitney test. *= P≤0.05; n=6 for both B7 and B27 samples. **(D)** Blood from B27 animals receiving the vehicle (CTRL) was collected twice a week for 4 weeks; numbers of CD43^{lo} and CCL2 plasma levels were measured for each sample. Samples were collected from 2 different experiments and results pooled. Correlation analysis was performed using Pearson r test. n=50. **(E)** Plasma was collected at different time points (day 1 to 26) from B27 and WT rats treated with ABX or water (CTRL) and CCL2 measured by ELISA. Plasma CCL2 of 3 different experiments pooled together in B27 rats and 1 experiment using WT. Error bars shown mean ± SD. In B27-CTRL n=9; in B27-ABX n=12; in WT-CTRL n=3; in WT-ABX n=3. Data were analysed using 2-way ANOVA and Sidak's multiple comparison test for repeated measure. *=P≤0.05; **=P≤0.005; ***=P≤0.0005. **(F)** IL-1α was measured in day 21 plasma samples from both WT and B27 groups. Error bars indicate mean ± SD of n=9-10 for B27 and n=3 for WT groups. Kruskal-Wallis test with Dunn's multiple comparisons test was used to assess the significance. **=

P≤0.01.

145x140mm (300 x 300 DPI)

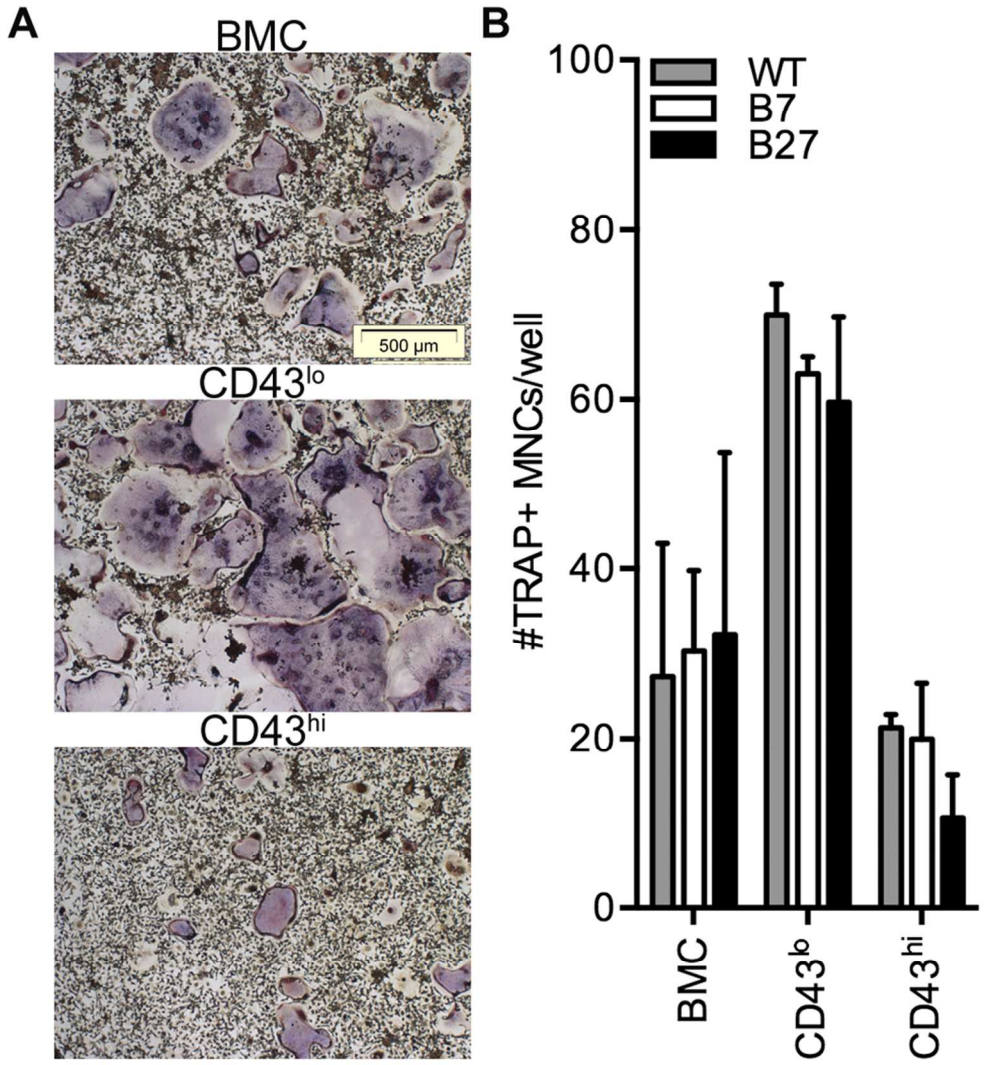

Figure 4. CD43^{lo} monocytes develop the highest number of osteoclasts *in vitro*. BMCs were collected from B7, B27 and WT rats and specific monocyte populations were sorted using flow cytometry. Sorted cells were cultured at the same density in pro-osteoclastogenic medium (50 ng/ml M-CSF and 50 ng/ml RANK-L) and after 7 days fixed and stained for TRAP. **(A)** Representative pictures of TRAP staining (purple staining) of the total BMCs and the different subpopulation analysed. Scale bar = 500µm **(B)** TRAP^{+} multinucleated (≥3 nuclei) cells (TRAP^{+} MNCs) were quantified as osteoclasts. Bars show mean ± SD. n=3 for WT, B7, and B27, from 3 different experiments pooled together.

83x88mm (300 x 300 DPI)

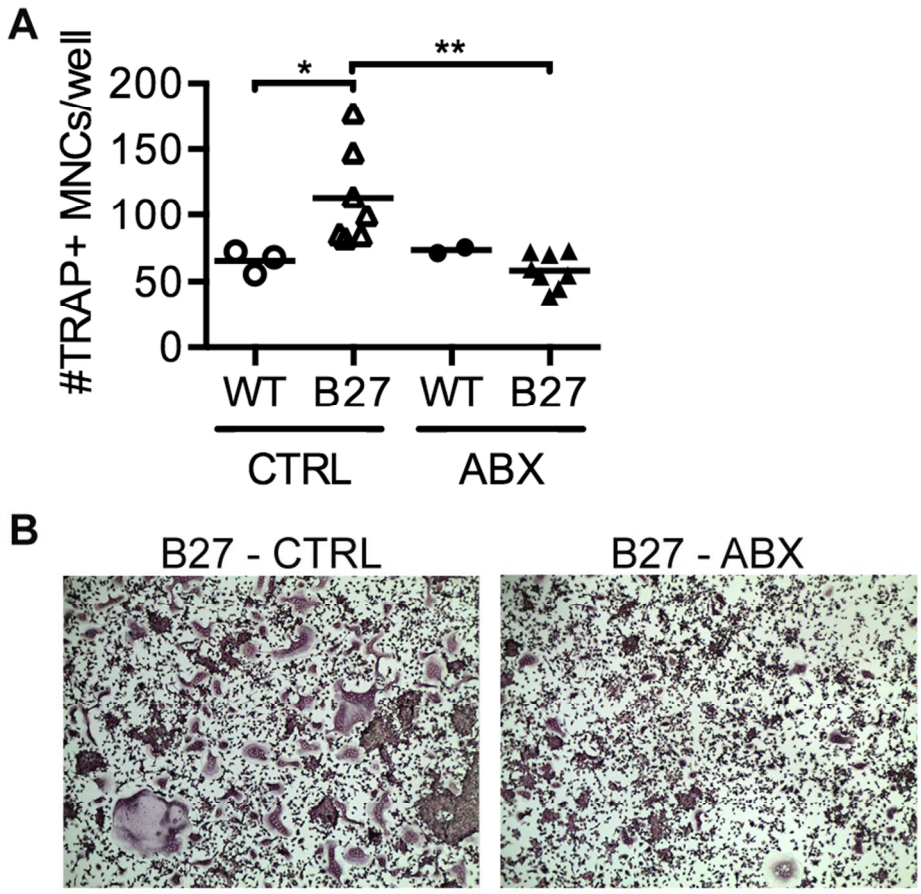

Figure 5. Antibiotics reverse the BM monocyte/osteoclast phenotype of B27 animals. B27 and WT animal received 4 weeks of ABX or water (CTRL) and at day 26 non-adherent-BMCs were collected and cultured in presence of 50 ng/ml M-CSF, 10 ng/ml RANK-L, and 50 ng/ml TNFα in triplicate wells. On day 4, medium was refreshed and on day 5 cells were fixed and stained for TRAP. Osteoclasts were quantified as $TRAP^+$ MNCs (≥3 nuclei) from 4 digital pictures per well. **(A)** The number of $TRAP^+$ MNCs deriving from culture of B27 and WT ABX and CTRL animals. Data in B27 derived from 2 different experiments pooled together for a total of n=7-8 for B27 and n=3 for WT. **(B)** Representative pictures show TRAP staining in a CTRL and ABX B27 cultures. Data were analysed with one-way ANOVA and Sidak's multiple comparison test. *=P≥0.05. **=P≥0.005.

83x75mm (300 x 300 DPI)